ISSN 1995-0780, Nanotechnologies in Russia, 2016, Vol. 11, Nos. 9–10, pp. 617–624. © Pleiades Publishing, Ltd., 2016.
Original Russian Text © A.S. Sizov, I.B. Meshkov, M.Yu. Yablokov, E.V. Agina, A.A. Bessonov, A.M. Muzafarov, S.A. Ponomarenko, 2016, published in Rossiiskie Nanotekhnologii, 2016, Vol. 11, Nos. 9–10.

# Molecular Silicasol-Based Barrier Coatings for Organic Electronics

**A. S. Sizov[a], I. B. Meshkov[a], M. Yu. Yablokov[a], E. V. Agina[a], A. A. Bessonov[b], A. M. Muzafarov[a, c], and S. A. Ponomarenko[a, d]***

[a] *Enikolopov Institute of Synthetic Polymeric Materials, Russian Academy of Sciences, Moscow, 117393 Russia*

[b] *Nokia Technologies, 21 JJ Thomson Avenue, Madingley Road, Cambridge CB3 0FA, United Kingdom*

[c] *Nesmeyanov Institute of Organoelement Compounds, Russian Academy of Sciences, Moscow, 119991 Russia*

[d] *Chemistry Department, Moscow State University, Moscow, 119991 Russia*

**e-mail: ponomarenko@ispm.ru*

Received February 1, 2016; in final form, June 14, 2016

**Abstract**—A solution-processable approach to designing molecular silicasol-based barrier coatings for organic electronics has been developed. The barriers are assessed by the optical calcium test and demonstrate water-vapor permeation rates of about $10^{-2}$ g m$^{-2}$ day$^{-1}$. Silicasols are shown to be promising for the encapsulation of organic electronics devices, for which the resulting water-vapor permeation rates are sufficient (e.g., for organic field-effect transistors).

**DOI:** 10.1134/S1995078016050189

## INTRODUCTION

Organic electronics is a field of science rapidly developing due to a promising potential for the design of cheap and flexible devices which can be produced only by solution processes [1]. A growing number of works in this field are dedicated to the industrial production of organic electronics devices, such as organic thin-film transistors (OTFT) [2, 3], organic light-emitting diodes (OLED) [4, 5], and organic solar cells [6, 7]. The charge carrier mobility in OTFT forming the basis of flexible chips has exceeded the corresponding values in amorphous silicon [8, 9]. However, one of the key factors restricting the spread of new-generation of light, flexible, and transparent (opto)electronic devices based on organic compounds is the problem of their degradation [10, 11].

Depending on the device type and architecture and materials used, the degradation problem is manifested in different ways and consists of deterioration in the values of key characteristics up to the total loss of functionality. For example, organic field-effect transistors are characterized by drops in the charge carrier mobility [12] and the on-off ratio [13], as well as by an increase in the threshold gate voltage [11]. Such degradation is caused by several factors, including the sensitivity of organic conductors and semiconductors to moisture and oxygen [14]. To provide desired protection of devices, several approaches have been applied, including the chemical modification of the semiconductor in order to control the level of highest occupied molecular orbital (HOMO) to decrease the possibility of their oxidation with air or water [15, 16]. Another approach, the kinetic barrier method, has gained the widest acceptance for n-type transistors. In such devices, the main charge carriers are electrons and, upon exposure to an external field, the semiconductor molecules form anions capable of reducing water and oxygen diffused into the semiconductor layer. The protection method consists of the search for organic semiconductive structures in the films of which diffusion into the active layer of the device is limited [17, 18]. The third approach consists of a deposition of an additional functional layer on a device where such a layer is a barrier coating preventing gas diffusion. Such protection is the most versatile and can be used for all types of organic electronic devices.

A great number of approaches to the design of barrier coatings have been developed to date. The deposition of glass- or metal-based coating on such devices to form an inert gas-filled laminating volume is the simplest method [19]. However, this approach is significantly limited, since it makes it impossible to design flexible devices using roll-to-roll processes. A promising alternative is the use of thin (20–40 nm) layers of metal and transition element oxides and nitrides, such as aluminum oxide ($Al_2O_3$) [20], silicon nitride ($Si_3N_4$) [21], and silicon dioxide ($SiO_2$) [22]. It is important that the increase in the thickness of such a coating does not allow significantly increasing its barrier properties. This is due to the presence of nanometer- and micron-sized defects formed at the initial step of film growth in the region of contact with the underlying functional layer. Such defects do not dis-

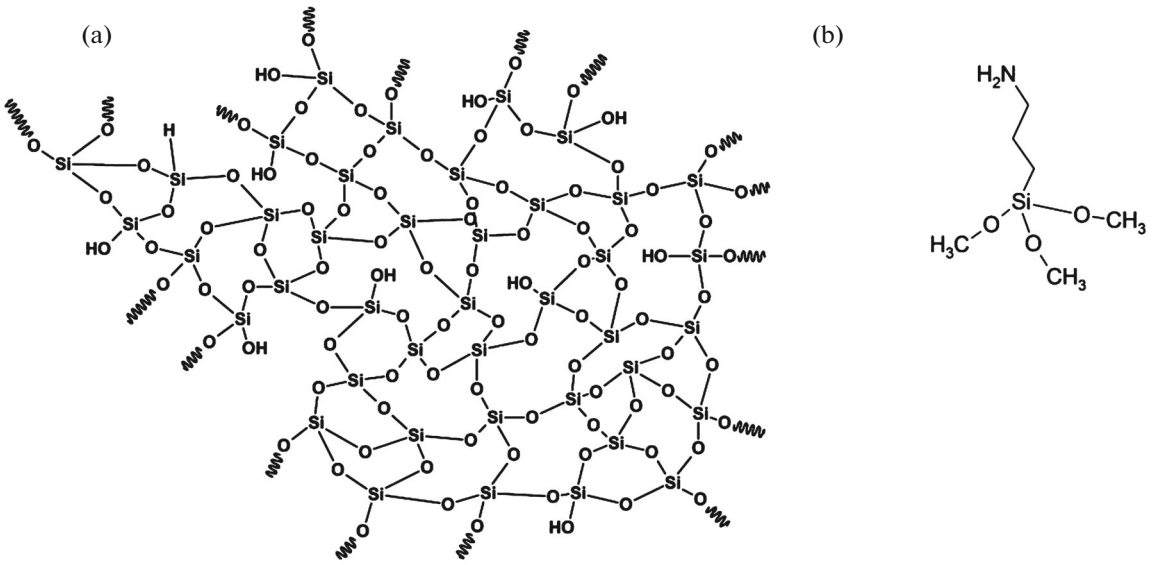


**Fig. 1.** Fragment of the hypothetic structural formula of molecular silicasol (a) and chemical formula of (3-aminopropyl)trimethoxysilane (APTMS) (b).

appear during film growth, but they form diffusion channels in the coating [23]. In addition, the processes for film fabrication include plasma treatment, ion sputtering, and chemical vapor deposition. This implies the treatment of the device surface with chemically and physically active components (plasma, chemical precursors, and solvents), which adversely affects the structure and properties of the underlying active layers of a device [24, 25]. Yet another approach consists of the use of a completely organic protective coating [26–29] providing its deposition above the active layer without a structural disturbance of the organic (semi)conductor. Such coatings demonstrate low barrier properties. Hybrid coatings where inorganic layers alternate with polymer ones were proposed as a compromise between the organic and inorganic coatings [30, 31]. This approach implies the alternation of vacuum and nonvacuum processes for film deposition, which increases the cost of films. In terms of ensuring a low cost of the final device, the most promising coatings are those prepared using only solution processing.

The aim of the present work was to develop a new solution-processable approach to the design of molecular silicasol-based barrier coatings that in the future can be used for the protection of flexible and transparent organic electronic devices.

## EXPERIMENTAL

A freshly prepared molecular silicasol was used as the basis for the preparation of barrier coatings; the fragment of its hypothetic structural formula is shown in Fig. 1a. Molecular silicasol [32] is a form of silica that can be dissolved in an anhydrous solvent, which in the present work was THF. Silicasol appears as individual nanoparticles with a size from several nanometers to dozens of nanometers, which is defined by its synthesis conditions. A distinctive feature of molecular silicasol is the adjustability of the ratio between its rigid polycyclic core and the more flexible edge, which results in a change in its state of aggregation from liquid to glassy solid [33, 34]. In the present work, we studied sufficiently rigid particles with a size of about 60 nm prepared according to the procedure published earlier [32]. Upon the deposition of nanoparticles onto the substrate surface, followed by keeping it in ammonia gas, individual particles can be cross-linked to form a single layer with a nanometer thickness. This approach provides the desired balance between the flexibility of a coating and its barrier properties.

The flexible substrate was a Teonex® Q65FA polyethylene naphthalate film (DuPont Teijin Films) with a thickness of 125 μm. This type of substrates was chosen because PEN is widely used in different applications of organic electronics [35]. The surface was pretreated by two methods: the first one uses treatment in the direct current plasma according to our procedure described earlier [36]. The second method consists of chemical modification of the substrate by the functional layer of (3-aminopropyl)trimethoxysilane (APTMS) (Fig. 1b) by gas-phase deposition [36]. The molecular silicasol-based barrier coating was deposited by spin coating at a rotational rate of 1000 rpm for 2 min and by dip coating.

The surface structure of barrier coatings was studied using an NT-MDT Solver NEXT atomic force microscope under semicontact conditions. Bruker NCHV-A cantilevers with a typical resonance frequency of 320 kHz, a curvature radius of 10 nm, and a stiffness of 42 N/m were used.

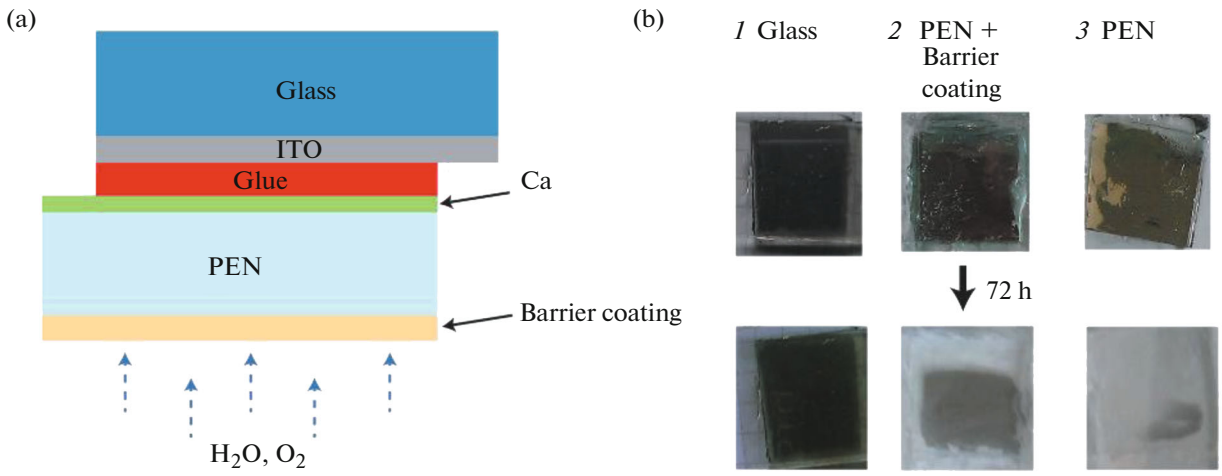


**Fig. 2.** (Color online) Schematic diagram of the optical calcium tests (a) and photographs of the samples with different protective coatings (b): (*1*) glass, (*2*) PEN + barrier coating, and (*3*) PEN. Photos were made immediately after the deposition of calcium (top row) and 72 h after being kept in air (bottom row).

The barrier properties were assessed by the optical calcium test [37], whose diagram is shown in Fig. 2a. The calcium layer with a thickness of 300–600 nm was deposited on the PEN surface with a barrier coating deposited on the opposite side. The resulting samples were attached to a glass with an ITO layer (20 × 20 mm) using a Done Deal DD6643 superglue in the argon atmosphere. Then, the dependence of the optical transmission of the calcium layer upon keeping in air was studied. The relative humidity was 60–70% and the temperature was 22°C. Calcium is oxidized (Fig. 2b) under the action of permeating water vapors and oxygen to form a transparent oxide. The gas permeability of the coating can be calculated by the kinetic equation of calcium layer oxidation

$$\frac{N(t)}{N_0} = 1 - S\omega t/m_{H_2O}, \quad (1)$$

where $N(t)$ is the number of calcium molecules at a time, $S$ is the area of coating, $m_{H_2O}$ is the weight of the water molecule, $t$ is time, and $\omega$ is the gas permeability

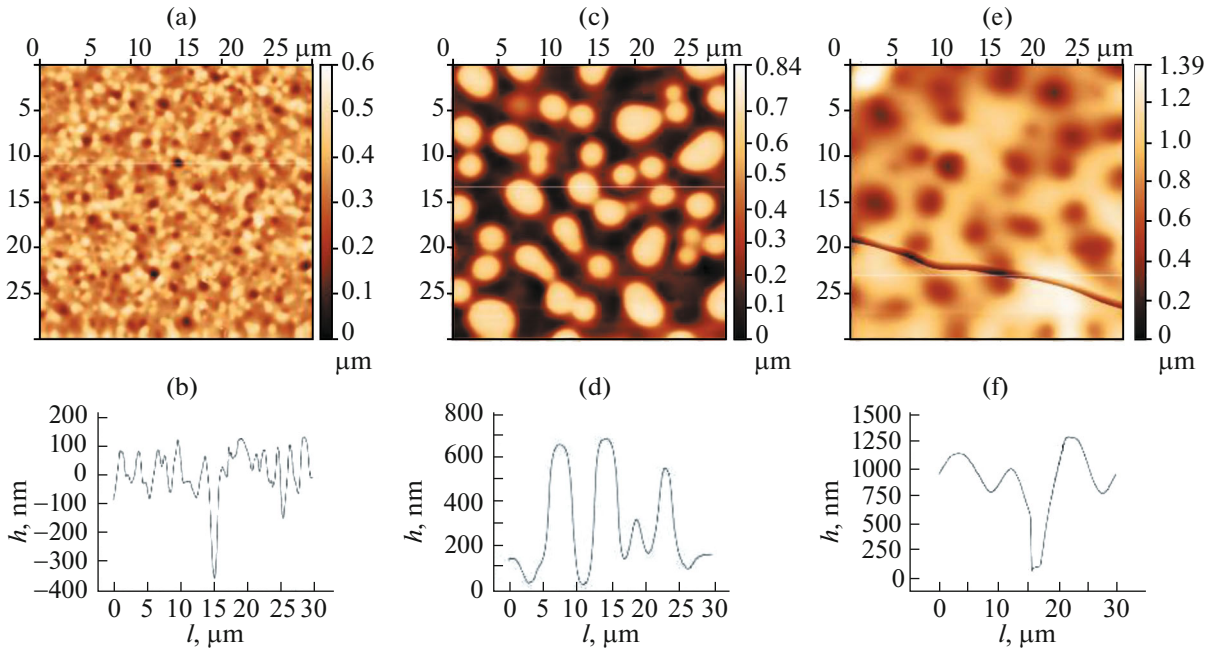


**Fig. 3.** (Color online) Results from the AFM study of silicasol-based coating without the pretreatment of the substrate surface: (a–d) surface morphology in different sections of the coating and the corresponding surface profiles; (e, f) surface morphology of the coating treated with ammonia and the corresponding surface profile.

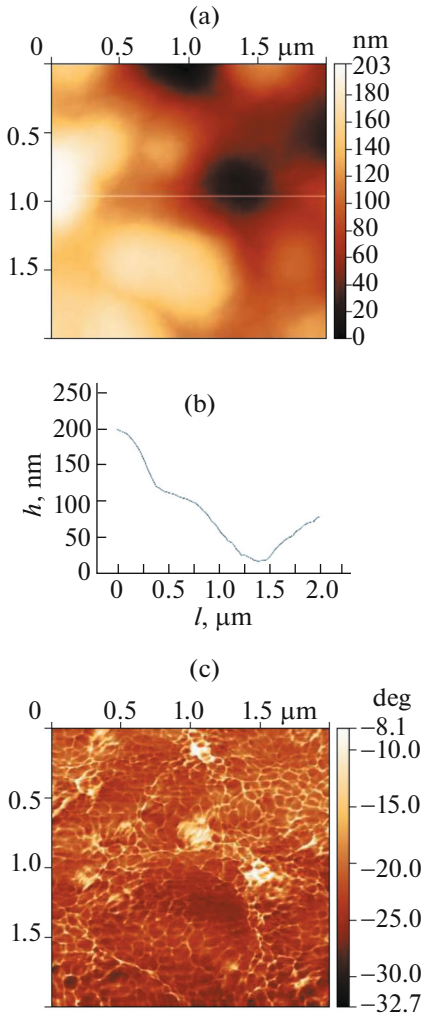


**Fig. 4.** (Color online) Results from the AFM study of silicasol-based coating without pretreatment of the substrate surface at small sizes of scanning region (2 μm): (a) film morphology, (b) corresponding surface profile, and (c) phase image.

of the coating. $N(t)$ was estimated by a calculation of the area of calcium visible on the photograph.

The calcium test was calibrated by gluing the ITO-containing glass to the deposited calcium. Calcium being between two glasses remained nontransparent for 4–5 weeks, which suggests an impermeability of the samples obtained and the applicability of this method to assess the gas-permeation rate of barrier coatings.

## RESULTS AND DISCUSSION

First, we studied the morphology of silicasol deposited on the PEN surface without additional treatment of the substrate. A dip-coated film was studied by atomic force microscopy (Fig. 3), which showed a high inhomogeneity in different regions of the substrate (Figs. 3a–3d). The typical roughness values varied from 70 to 200 nm and the surface appeared as a layer of particles whose lateral size distribution in different sections of the substrate changed from 1 to 5 μm. Upon cross linking this film with ammonia, the coating inhomogeneity remained unchanged (Figs. 3e, 3f). In addition, due to the large film thickness in some regions of the sample, cross linking resulted in a fragility of the layer, which, in turn, resulted in the formation of macro cracks. Thus, the increase in the homogeneity of the coating prior to its cross linking becomes of current concern.

In order to study in more detail the structure of coating surface, the AFM studies on scanned regions with a size of 2 μm were performed. Neither the 2D height image of surface topology (Fig. 4a) nor its profile (Fig. 4b) allows one to see its fine structure, while the corresponding 2D phase image (Fig. 4c) shows that microparticles consist of individual nanoparticles with sizes from 50 to 100 nm. This size distribution is close to that obtained for this solution of molecular silicasol by small-angle X-ray scattering [32]. Thus, the molecular silicasol film on the polymer substrate is clusters of individual nanoparicles; the particle size distribution is quite wide. The gaps formed in this coating significantly decrease the effective film thickness, which, over the long term, will have an adverse effect on the gas permeation rate.

There are a number of surface pretreatment methods providing an increase in the surface adhesion, such as keeping of a substrate in plasma or treatment with a modifying agent, which results in a more homogeneous particle size distribution over the surface. The efficiency of the abovementioned approaches was studied systematically in the present work. Figure 5 shows the surface morphology of the silicasol layer deposited on the plasma-pretreated substrate according to the AFM data. The film is macroscopically homogeneous with a roughness of RMS = 14 nm. One important fact is that individual nanoparticles with sizes from 50 to 100 nm were observed upon the study of the film thin structure analogously to the plasma-untreated sol film. Subsequent treatment of the film in ammonia has a slight effect on the film structure on a macroscale; however, the traces of nanoparticles in a microstructure disappear, which results in a significant planarization of the surface (RMS decrease to 8 nm) (Fig. 5d) and individual nanoparticles become to be indistinguishable (Fig. 5f). This suggests that individual particles undergo cross linking to form a single coating. The homogeneity of the resulting film implies that the film has high barrier properties.

Figure 6 shows the silicasol film deposited on the (3-aminopropyl)trimethoxysilane (APTMS)-pretreated substrate. In contrast to the coating obtained on the plasma-pretreated substrate, this coating has a cluster structure similar to that obtained for the coating on the nonpretreated substrate with a cluster size of 0.5–0.7 μm. In addition, the pretreatment with

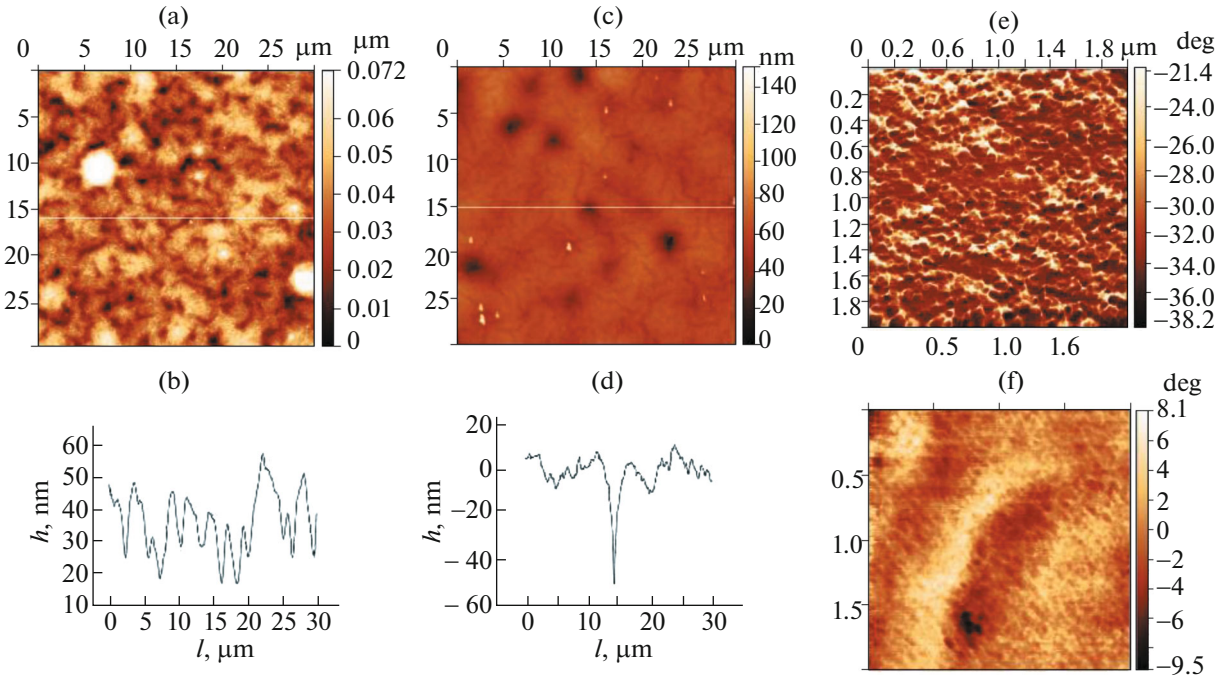


**Fig. 5.** (Color online) Results from an AFM study of silicasol-based coating deposited on the plasma-pretreated substrate: surface morphology prior to (a) and after (c) ammonia treatment, (b, d) corresponding surface profiles, and (e) phase signal prior to ammonia treatment and (f) after ammonia treatment.

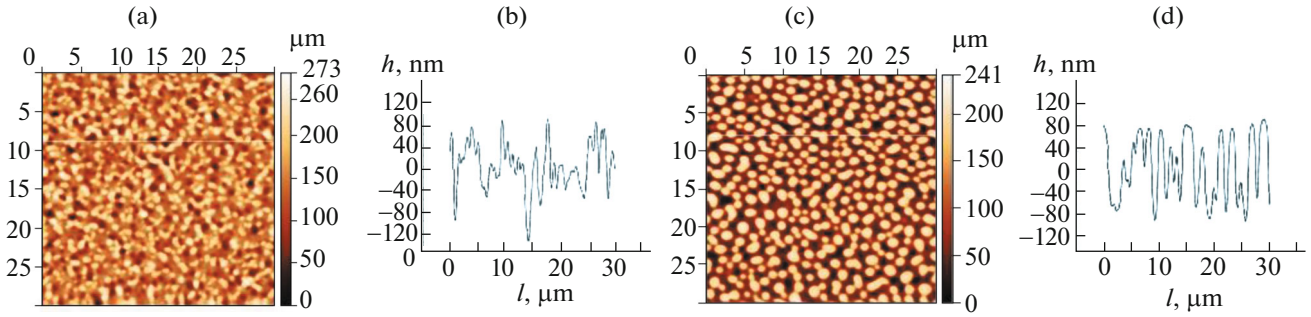


**Fig. 6.** (Color online) AFM-studied morphology of the molecular silicasol film deposited on APTS-pretreated substrate prior to (a) and after (b) ammonia treatment; (c, d) corresponding surface profiles.

APTMS allowed significantly increasing the homogeneity of the coating (the particle size distributions in different regions of the sample are identical), which makes this film a promising basis for barrier coatings. After being kept in ammonia gas, the film morphology deteriorated; namely, some nanoparticles coagulated into coarser ones (1–3 μm). Based on the data, one can conclude that ammonia pretreatment is not a promising procedure to improve the coating quality in the case when polymer is pretreated with APTMS.

In the present work we also compared the methods of coating deposition on the polymer substrate. Figure 7a shows the surface morphology of spin-coated silicasol film deposited from a solution in THF on the APTMS-pretreated polymer surface. The film is highly homogeneous on a macroscale; however, it contains nanopores with a radius of 50–100 nm. Similar pores were observed upon the spin-coating deposition of silica sol on the plasma-pretreated polymer (Fig. 7b). The problem of formation of such pores is well known and often solved by the deposition of a coating from a high-boiling solvent. This approach allows one to balance the kinetics of solvent evaporation and film formation. The silicasol-based coating was deposited from such high-boiling solvent as diglyme (diethylene glycol dimethyl ether). Its surface morphology (Fig. 7c) is also highly homogeneous on a macroscale; the pore density decreased by one to two

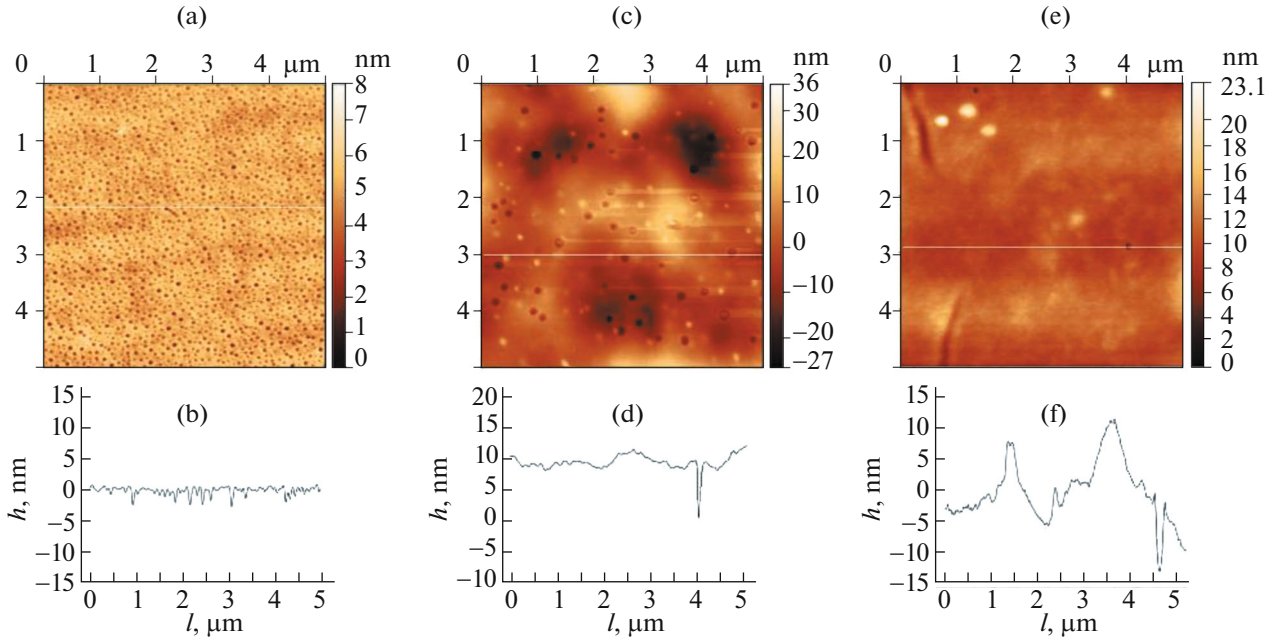


**Fig. 7.** (Color online) AFM-studied morphology of the spin-coated silicasol film deposited on the substrate pretreated with APTMS (a) and plasma (c) from THF, as well as on the substrate pretreated with APTMS from the high-boiling solvent (diglyme) (e); (b, d, f) corresponding surface cross sections.

orders of magnitude. This coating must be more promising in terms of barrier properties; for this reason it was assessed by the optical calcium test along with the best coatings obtained by other methods considered above.

Figure 8 shows the results from the optical calcium test of coatings for gas permeating rates. All coatings, as well as the coatingless substrate, showed that the portion of unoxidized calcium depends linearly on the time. Based on the experimental data, the gas permeation rates ω were calculated approximating formula 1 by the least-squares method.

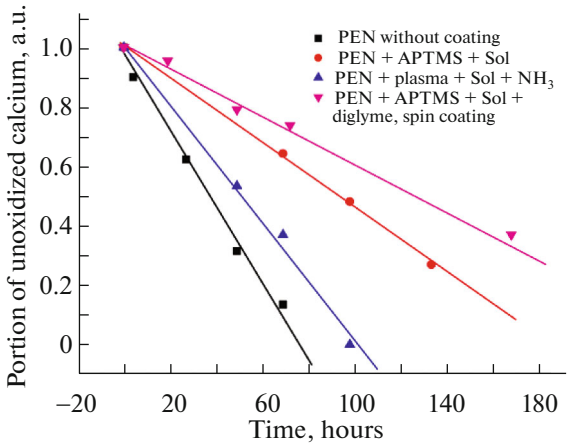


**Fig. 8.** (Color online) Results from optical calcium tests of coatings for gas permeation rates.

The table gives a comparison between the properties of silicasol-based coatings obtained by different methods. It should be noted that both methods proposed for the surface pretreatment (plasma and APTMS) provided a macroscopic homogeneity of the surface, as well as low values of roughness, which suggests that coatings have high barrier properties. Solution deposition allows one to design a coating consisting of individual nanoparticles with sizes from 50 to 100 nm regardless of the pretreatment method. Upon the subsequent cross-linking of silicasol with ammonia, the visible traces of nanoparticles disappear, which suggests the formation of a continuous coating. The gas permeation rate of silicasol deposited on the APTMS layer was found to be almost twofold lower than that of the plasma-pretreated coating ($2.5 \times 10^{-2}$ g m$^{-2}$ day$^{-1}$ versus $4.6 \times 10^{-2}$ g m$^{-2}$ day$^{-1}$, respectively). This result correlates with the results from the AFM study of the coatings according to which the layer on the APTMS-containing substrate is a homogeneous film with a small number of defects. In the case of spin coating method with different pretreatment techniques, no traces of nanoparticles in the film structure were detected. The use of a high-boiling solvent (diglyme) allowed us to obtain a highly homogeneous coating with a measured gas permeation rate of $2.1 \times 10^{-2}$ g m$^{-2}$ day$^{-1}$. This value is close to that for the coating deposited on the APTMS layer. It should be noted that all deposition and pretreatment methods showed gas permeation rates have the same order of magnitude ($10^{-2}$ g m$^{-2}$ day$^{-1}$) and the best result was obtained by spin coating, which pro-

Comparison between the properties of molecular silicasol-based barrier coatings obtained by different methods

| | Coating type | Roughness, nm | Macroscopic homogeneity of coating | Cluster size, μm | Nanoparticle size, nm | Water vapor permeation rate, g $m^{-2}$ $day^{-1}$ |
|---|---|---|---|---|---|---|
| | PEN | 1–2 | – | – | – | $6.5 \times 10^{-2}$ |
| Dip coating | PEN + Sol | 70–200 | No | 1–5 | 50–100 | – |
| | PEN + plasma + Sol | 15 | Yes | – | 50–100 | – |
| | PEN + plasma + Sol + $NH_3$ | 8 | Yes | – | – | $4.6 \times 10^{-2}$ |
| | PEN + APTMS + Sol | 25 | Yes | 0.5–0.7 | 50–100 | $2.5 \times 10^{-2}$ |
| | PEN + APTMS + Sol + $NH_3$ | 50 | Yes | 1–3 | – | – |
| Spin coating | PEN + plasma + Sol | 5 | Yes | – | – | – |
| | PEN + APTMS + Sol | 1.8 | Yes | – | – | – |
| | PEN + APTMS + Sol **(diglyme)** | 1.8 | Yes | – | – | $2.1 \times 10^{-2}$ |

vided a threefold increase in the complete oxidation time.

## CONCLUSIONS

A novel approach to the design of barrier coatings based on molecular silicasol was developed using exclusively solution processing. Molecular silicasol was shown to be a promising basis for barrier coatings on organic electronics due to a combination of acceptable water-vapor permeation rates with an ease of fabrication. Such coatings can be deposited using only solution processes, in contrast to a great number of already existing approaches. The most homogeneous silicasol films were assessed by the optical calcium test to show water-vapor permeation rates of about $10^{-2}$ g $m^{-2}$ $day^{-1}$. The spin-coated molecular silicasol deposited on the APTMS-pretreated surface from the high-boiling solvent demonstrated the best results. Thus, silicasols can be used to encapsulate organic electronics devices for which the resulting water vapor permeation rates are sufficient (e.g., organic field-effect transistors) [38].

## ACKNOWLEDGMENTS

This work was financially supported by Nokia Corporation and RFBR (project no. 14-03-00873).

## REFERENCES

1. S. R. Forrest, Nature **428** (6986), 911–918 (2004).
2. S. Yang, C. S. Hwang, J. I. Lee, S. M. Yoon, M. K. Ryu, K. I. Cho, S. H. K. Park, S. H. Kim, C. E. Park, and J. Jang, Appl. Phys. Lett. **98** (10), 103515 (2011).
3. H. Klauk, Chem. Soc. Rev. **39** (7), 2643–2666 (2010).
4. L. X. Xiao, Z. J. Chen, B. Qu, J. X. Luo, S. Kong, Q. H. Gong, and J. J. Kido, Adv. Mater. **23** (8), 926–952 (2011).
5. T. H. Han, Y. Lee, M. R. Choi, S. H. Woo, S. H. Bae, B. H. Hong, J. H. Ahn, and T. W. Lee, Nat. Photon. **6** (2), 105–110 (2012).
6. T. Stubhan, M. Salinas, A. Ebel, F. C. Krebs, A. Hirsch, M. Halik, and C. J. Brabec, Adv. Energy Mater. **2** (5), 532–535 (2012).
7. J. Min, Y. N. Luponosov, N. Gasparini, M. Richter, A. V. Bakirov, M. A. Shcherbina, S. N. Chvalun, L. Grodd, S. Grigorian, T. Ameri, S. A. Ponomarenko, and C. J. Brabec, Adv. Energy Mater. **5** (17), 1500386 (2015).
8. T. W. Kelley, L. D. Boardman, T. D. Dunbar, D. V. Muyres, M. J. Pellerite, and T. Y. P. Smith, J. Phys. Chem. B **107** (24), 5877–5881 (2003).
9. C. D. Dimitrakopoulos and P. R. L. Malenfant, Adv. Mater. **14** (2), 99 (2002).
10. H. Sirringhaus, Adv. Mater. **21** (38–39), 3859–3873 (2009).
11. P. A. Bobbert, A. Sharma, S. G. J. Mathijssen, M. Kemerink, and D. M. de Leeuw, Adv. Mater. **24** (9), 1146–1158 (2012).
12. Q. Xia, M. Burkhardt, and M. Halik, Org. Electron. **9** (6), 1061–1068 (2008).
13. L. Torsi, A. Dodabalapur, N. Cioffi, L. Sabbatini, and P. G. Zambonin, Sens. Actuators B **77** (1–2), 7–11 (2001).
14. L. H. Kim, K. Kim, S. Park, Y. J. Jeong, H. Kim, D. S. Chung, S. H. Kim, and C. E. Park, ACS Appl. Mater. Interfaces **6** (9), 6731–6738 (2014).
15. D. M. de Leeuw, M. M. J. Simenon, A. R. Brown, and R. E. F. Einerhand, Synth. Met. **87** (1), 53–59 (1997).
16. T. D. Anthopoulos, G. C. Anyfantis, G. C. Papavassiliou, and D. M. de Leeuw, Appl. Phys. Lett. **90** (12), 122105 (2007).
17. Z. A. Bao, A. J. Lovinger, and J. Brown, J. Am. Chem. Soc. **120** (1), 207–208 (1998).
18. H. E. Katz, J. Johnson, A. J. Lovinger, and W. J. Li, J. Am. Chem. Soc. **122**, 7787–7792 (2000).
19. P. E. Burrows, V. Bulovic, S. R. Forrest, L. S. Sapochak, D. M. Mccarty, and M. E. Thompson, Appl. Phys. Lett. **65**, 2922–2924 (1994).

20. C. Charton, N. Schiller, M. Fahland, A. Hollander, A. Wedel, and K. Noller, Thin Solid Films **502**, 99–103 (2006).
21. D. A. Spee, J. K. Rath, and R. E. I. Schropp, Thin Solid Films **575**, 67–71 (2015).
22. A. Perrotta, E. R. J. van Beekum, G. Aresta, A. Jagia, W. Keuning, R. M. C. M. van de Sanden, E. W. M. M. Kessels, and M. Creatore, Microporous Mesoporous Mater. **188**, 163–171 (2014).
23. A. P. Roberts, B. M. Henry, A. P. Sutton, C. R. M. Grovenor, G. A. D. Briggs, T. Miyamoto, A. Kano, Y. Tsukahara, and M. Yanaka, J. Membr. Sci. **208** (1–2), 75–88 (2002).
24. F. L. Wong, M. K. Fung, S. L. Tao, S. L. Lai, W. M. Tsang, K. H. Kong, W. M. Choy, C. S. Lee, and S. T. Lee, J. Appl. Phys. **104** (1), 014509 (2008).
25. S. Nam, H. Jeon, S. H. Kim, J. Jang, C. Yang, and C. E. Park, Org. Electron. **10** (1), 67–72 (2009).
26. D. Feili, M. Schuettler, T. Doerge, S. Kammer, and T. Stieglitz, Sens. Actuators A: Phys. **120** (1), 101–109 (2005).
27. C. D. Sheraw, L. Zhou, J. R. Huang, D. J. Gundlach, T. N. Jackson, M. G. Kane, I. G. Hill, M. S. Hammond, J. Campi, B. K. Greening, J. Francl, and J. West, Appl. Phys. Lett. **80** (6), 1088 (2002).
28. H. Jung, T. Lim, Y. Choi, M. Yi, J. Won, and S. Pyo, Appl. Phys. Lett. **92** (16), 163504 (2008).
29. X. Yan, H. Wang, and D. Yan, Thin Solid Films **515** (4), 2655–2658 (2006).
30. G. L. Graff, R. E. Williford, and P. E. Burrows, J. Appl. Phys. **96** (4), 1840–1849 (2004).
31. M. S. Weaver, L. A. Michalski, K. Rajan, M. A. Rothman, J. A. Silvernail, J. J. Brown, P. E. Burrows, G. L. Graff, M. E. Gross, P. M. Martin, M. Hall, E. Mast, C. Bonham, W. Bennett, and M. Zumhoff, Appl. Phys. Lett. **81**, 2929–2931 (2002).
32. RF Patent No. 2140393 (1999).
33. N. V. Voronina, I. B. Meshkov, V. D. Myakushev, N. V. Demchenko, T. V. Laptinskaya, and A. M. Muzafarov, Nanotechnol. Russ. **3**, 321 (2008).
34. N. V. Voronina, I. B. Meshkov, V. D. Myakushev, T. V. Laptinskaya, V. S. Papkov, M. I. Buzin, M. N. Il'ina, A. N. Ozerin, and A. M. Muzafarov, J. Polym. Sci. Polym. Chem. **48** (19), 4310–4322 (2010).
35. T. Sekitani and T. Someya, Mater Today **14** (9), 398–407 (2011).
36. E. V. Agina, A. S. Sizov, M. Y. Yablokov, O. V. Borshchev, A. A. Bessonov, M. N. Kirikova, M. J. A. Bailey, and S. A. Ponomarenko, ACS Appl. Mater. Interface **7** (22), 11755–11764 (2015).
37. D. J. Higgs, M. J. Young, J. A. Bertrand, and S. M. George, J. Phys. Chem. C **118**, 29322–29332 (2014).
38. "Reel-to-reel vacuum metallization," in *Organic Electronics: Materials, Manufacturing, and Applications,* Ed. by H. Klauk (Wiley-VCH, 2006), Chap. 8.

*Translated by K. Utegenov*